algorithms

MDPI

Article

An Approach for Setting Parameters for Two-Degree-of-Freedom PID Controllers

Xinxin Wang [1], Xiaoqiang Yan [1,*], Donghai Li [2] and Li Sun [3]

[1] School of Mechanical Engineering, University of Science and Technology Beijing, Beijing 100083, China; wangxinxin404@163.com
[2] State Key Lab of Power Systems, Department of Thermal Engineering, Tsinghua University, Beijing 100084, China; lidongh@mail.tsinghua.edu.cn
[3] Key Lab of Energy Thermal Conversion and Control of Ministry of Education, Southeast University, Nanjing 210096, China; sunli12@seu.edu.cn
* Correspondence: yanxq@ustb.edu.cn; Tel.: +86-186-0026-0898

Received: 19 March 2018; Accepted: 6 April 2018; Published: 13 April 2018

Abstract: In this paper, a new tuning method is proposed, based on the desired dynamics equation (DDE) and the generalized frequency method (GFM), for a two-degree-of-freedom proportional-integral-derivative (PID) controller. The DDE method builds a quantitative relationship between the performance and the two-degree-of-freedom PID controller parameters and guarantees the desired dynamic, but it cannot guarantee the stability margin. So, we have developed the proposed tuning method, which guarantees not only the desired dynamic but also the stability margin. Based on the DDE and the GFM, several simple formulas are deduced to calculate directly the controller parameters. In addition, it performs almost no overshooting setpoint response. Compared with Panagopoulos' method, the proposed methodology is proven to be effective.

Keywords: two-degree-of-freedom PID; the desired dynamics equation; the generalized frequency method; stability margin

1. Introduction

The proportional-integral-derivative (PID) controller, which is by far the most common control algorithm, is widely used in the industry due to its simplicity and ease of tuning [1,2]. It is well-known that PID controllers can be implemented in two forms: single-degree-of-freedom (1-DOF) PID and two-degree-of-freedom (2-DOF) [3]. Because the design of the control system can be seen as a multi-objective optimization [4], and because there is a trade-off between the setpoint response and the load disturbance attenuation in the 1-DOF PID structure [5,6], the 2-DOF PID structure was proposed [7]. Due to its superiority, the 2-DOF PID has drawn great attention from many researchers, and a great number of tuning methods have been proposed, such as the dominant poles method [8,9], the internal model control (IMC) [10–12], the gain–phase margin method (GPM) [13], the maximum sensitivity method [14,15], the desired dynamic equation method (DDE) [16–18], etc.

The tuning method proposed is an improvement of the DDE method. The DDE is a 2-DOF tuning method based on the desired dynamic, disturbance estimate, and disturbance compensation. The DDE method has the following advantages. On the one hand, it endows the controller parameters with physical meanings [19,20], because it can build the equivalent relationship between the 2-DOF PID structure and the Tornambe controller (TC) [21] structure, which is characterized by clear physical meanings. On the other hand, due to the equivalent relationship between the 2-DOF PID structure and the TC, the DDE makes the parameter settings of the 2-DOF PID not dependent on a precise model [22,23]. The nature of the TC is that a disturbance observer estimates the total disturbance and then dynamically compensates it; therefore, the model error can be seen as an internal disturbance that is estimated and then compensated. However, the major drawback of the DDE method is that the stability margin cannot be guaranteed. So, we propose using the generalized frequency method (GFM) in addition to the DDE method, because this DDE–GFM can guarantee both the desired dynamic and the stability margin [24].

The GFM can guarantee the stability margin by limiting the closed-loop poles to a stability sector area in the left half-plane. What is more, it can not only accurately guarantee the specified stability margin by only one parameter but also calculate the controller parameter directly and analytically, whereas M_s (the maximum sensitivity) and GPM cannot realize these two purposes simultaneously. In addition, the GFM has been used to set single-degree-of-freedom PID parameters [25]. Thus, the GFM has been chosen to be the stability margin criterion.

In [24,25], the GFM builds the relationship between the controller parameters and the stability margin. Moreover, it is known that the DDE method builds the relationship between the 2-DOF PID and the TC, and the TC builds the relationship between the controller parameters and the desired dynamic. So, the desired dynamic, represented as the controller parameters h_0 and h_1, and the stability margin, represented as the controller parameter m, can be specified. Then, a contour, characterized by the same m, h_0, and h_1, is obtained. In the contour, an appropriate work point is derived to calculate the controller parameters. Finally, an appropriate work point to calculate the controller parameters can be obtained. This is the principle of the DDE–GFM.

The tuning steps of the DDE–GFM are briefly shown as follows. It is known that the parameters of the 2-DOF PID (k_p, k_i, k_d, b) have been converted into the parameters of the TC (h_0, h_1, k, l) according to the DDE. Firstly, h_0, h_1, and m are specified based on the desired dynamic and the stability margin, then k and l are converted into $1/l$ and k/l. Next, the contour is depicted in the $(k/l, 1/l)$ plane, restraining the stability margin with the GFM. Finally, an appropriate work point is derived, which possesses a big enough k to improve the estimation of the total disturbance to calculate the controller parameters.

The proposed method not only guarantees the desired dynamic but also the stability margin. Moreover, several simple formulas were deduced to calculate directly the controller parameters. In addition, it performs almost no overshooting setpoint response because the desired dynamic is in critically damped system. Compared with Panagopoulos' method [15], the settling time is shortened and the overshooting is drastically decreased, while the maximum sensitivity stays the same.

This paper is organized as follows. Section 2 describes the related tuning methods (i.e., the desired dynamics equation method and the generalized frequency method) and the steps of setting the controller parameters. Section 3 offers some examples with simulations to illustrate the analysis of the controller parameters in detail. A comparison with Panagopoulos' method is also included in this section. Section 4 is the conclusion.

2. The Related Tuning Methods

2.1. The Desired Dynamics Equation (DDE) Method

Consider the transfer function given by:

$$G_p(s) = \frac{\sum\limits_{i=0}^{r} b_i s^i}{\sum\limits_{j=0}^{n} a_j s^j} \tag{1}$$

where a_j and b_i are unknown parameters. It can be transformed to the following state space form:

$$\begin{cases} \dot{z}_1 = z_2 \\ \dot{z}_2 = f\left(z_1, z_2, \cdots, z_n, u, \dot{u}, \cdots, u^{(r)}\right) + lu \\ y = z_1 \end{cases} \tag{2}$$

where $u, \dot{u}, \cdots, u^{(r)}$ are the plant input and its derivatives; y is the plant output; $z_1, z_2, \cdots, z_n$ are the system states; l is a proper positive constant number; and $f\left(z_1, z_2, \cdots, z_n, u, \dot{u}, \cdots, u^{(r)}\right)$ is the total disturbance.

The desired dynamic equation is as follows:

$$\frac{Y(s)}{R(s)} = \frac{h_0}{s^2 + h_1 s + h_0} \tag{3}$$

To reach Equation (3), the corresponding control law should be:

$$u = \left[-h_0(z_1 - y_r) - h_1 z_2 - \hat{f}\right]/l \tag{4}$$

where h_0 and h_1 are the coefficient of the desired dynamic and are determined by the requirements of the control system; and $\hat{f}$ is the estimation of total disturbance $f\left(z_1, z_2, \cdots, z_n, u, \dot{u}, \cdots, u^{(r)}\right)$.

To obtain the estimation of total disturbance $\hat{f}$, the following disturbance observer is used.

$$\begin{cases} \hat{f} = \xi + k z_2 \\ \dot{\xi} = -k\xi - k^2 z_2 - klu \end{cases} \tag{5}$$

where k is the coefficient of the disturbance observer and indicates the speed of tracking disturbance; and ξ is an intermediate variable.

Equation (5) structures a disturbance observer. Equation (4) offers the control law to achieve the desired dynamic Equation (3). The disturbance observer estimates the total disturbance and compensates the systems to be the desired dynamic in real time and dynamically.

By substituting Equations (2), (3) and (5) into Equation (4), we can obtain

$$u = \frac{(h_0 + kh_1)e + kh_0 \int edt + (h_1 + k)\dot{e} - kh_1 y_r}{l} \tag{6}$$

where y_r is the target value; and e is the error between the plant output and the target value. The detailed derivation is shown in Appendix A.

From Equation (6), we can obtain the two-degree-of-freedom PID controller parameters,

$$\begin{cases} k_p = (h_0 + kh_1)/l \\ k_i = kh_0/l \\ k_d = (h_1 + k)/l \\ b = kh_1/l \end{cases}. \tag{7}$$

The corresponding two-degree-of-freedom PID controller structure is shown in Figure 1.

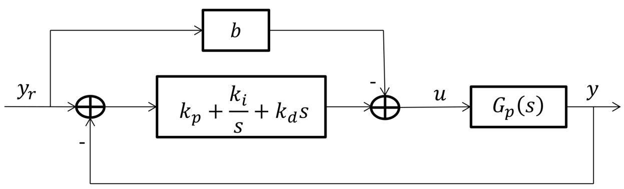

Figure 1. Two-degree-of-freedom proportional-integral-derivative (PID) controller structure.

When the desired dynamic equation is as follows:

$$\frac{Y(s)}{R(s)} = \frac{h_0}{s + h_0}, \tag{8}$$

we can analogously obtain the two-degree-of-freedom PID controller parameters,

$$\begin{cases} k_p = (h_0 + k)/l \\ k_i = kh_0/l \\ b = k/l \end{cases} . \tag{9}$$

In general, the DDE endows the 2-DOF PID controller parameters with clear physical meaning, which makes some of the parameters specified and then decreases the number of unknown parameters. Moreover, the model error is imposed into the total disturbance and is compensated, so the precise model is not necessary.

2.2. Generalized Frequency Method (GFM)

The GFM can calculate the controller parameters directly and analytically and can accurately guarantee the specified stability margin with only one parameter, which is called the attenuation index m. The attenuation index m determines the two rays, which shape a sector area shown in Figure 2, and the GFM can make all the closed-loop poles lie in the resulting sector area. The equation of the two rays is $s = -|m\omega| + j\omega$, where $m > 0$, $m = \tan\alpha$. m is a constant and α is the included angle between the ray and the imaginary axis.

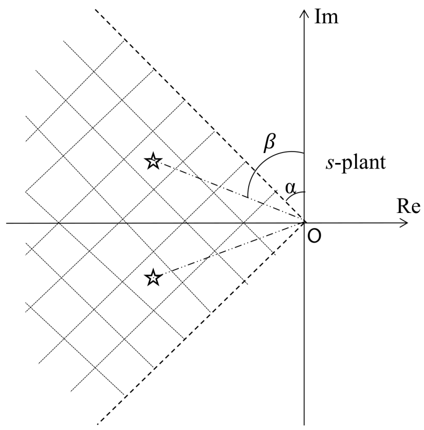

Figure 2. Generalized frequency characteristic.

The stability margin increases with attenuation index m. Each pair of conjugate complex poles have a corresponding m_n, $m_n = \tan\beta$ and the corresponding m_n equal to infinity for the real poles. The minimum m_n is equal to the specified attenuation index m, i.e., $\min\{m_n\} = m$.

Next, we will illustrate the relationship between the maximum sensitivity (M_s) and the attenuation index m to explain the rationality of the attenuation index m as the stability margin criterion. $G(s) = 1/(s+1)^4$ is taken as an example. Substitute $s = -m\omega + j\omega$ into $G(s)$, and the Nyquist plots of $m = 0, 0.1, 0.2$ are shown in Figure 3.

In Figure 3, the Nyquist plots are shown with full lines, and $m = 0$, $m = 0.1$, and $m = 0.2$ are respectively shown with a red line, green line, and blue line; dashed lines represent the maximum sensitivity $M_s = 1/R$ and the dashed red line, green line, and blue line respectively represent R_0, R_1, and R_2. The stability margin of $G(-m\omega + j\omega)$ decreases with the attenuation index m increasing. So, when designing the controller parameters, make the transfer function $G(-m\omega + j\omega)C(-m\omega + j\omega)$ to give $G(j\omega)C(j\omega)$ as the stability margin, where C represents the transfer function of the controller. From above, the attenuation index m can give a system stability margin in parameter design stage, and thus, it can be a stability margin criterion.

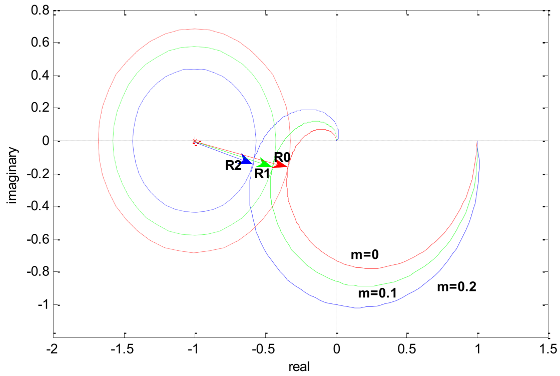

Figure 3. The relation between the maximum sensitivity M_s and the attenuation index m in Nyquist plots.

2.3. Setting PID Controllers Parameters

In this subsection, first a set of tuning equations is derived, and then, controller parameters are analyzed. Finally, the steps of the tuning method are given.

For the control system in Figure 1, its stability is determined by the closed-loop characteristic equation:

$$1 + (k_p + k_i/s + k_d s)G_p(s) = 0. \tag{10}$$

Substitute $s = -m\omega + j\omega$ into Equation (10), define $G_p(-m\omega + j\omega) = M_0(m,\omega)e^{j\varphi_0(m,\omega)}$, and compare the real and imaginary parts; the following equation is obtained

$$\begin{cases} k_p = -\frac{1}{M_0(m,\omega)}\begin{bmatrix} m\sin\varphi_0(m,\omega) \\ +\cos\varphi_0(m,\omega) \end{bmatrix} + 2m\omega k_d \\ k_i = \omega(1+m^2)\left[\omega k_d - \frac{1}{M_0(m,\omega)}\sin\varphi_0(m,\omega)\right] \end{cases} \tag{11}$$

Under certain m, Equation (11) structures a marginal stability surface with various ω. The marginal stability surface divides the (k_p, k_i, k_d) space into two parts: meeting stability margin and not meeting stability margin.

Employing the following variable substitution,

$$\begin{cases} p = 1/l \\ q = k/l \end{cases}, \tag{12}$$

Equation (7) is expressed as

$$\begin{cases} k_p = h_0 p + h_1 q \\ k_i = q h_0 \\ k_d = p h_1 + q \\ b = q h_1 \end{cases}. \tag{13}$$

Substitute Equation (13) into Equation (11), and the following equation is obtained

$$\begin{cases} (h_1 - 2m\omega)q + (h_0 - 2m\omega h_1)p \\ = -\frac{m\sin\varphi_0(m,\omega)+\cos\varphi_0(m,\omega)}{M_0(m,\omega)} \\ \left[h_0 - \omega^2(1+m^2)\right]q - \omega^2(1+m^2)h_1 p \\ = -\frac{\omega(1+m^2)\sin\varphi_0(m,\omega)}{M_0(m,\omega)} \end{cases}. \tag{14}$$

Under certain h_0, h_1, m and ω, Equation (14) becomes a linear equation. Then, if its Jacobian determinant J is nonsingular, it has a unique local solution (q, p). Under various ω and certain h_0, h_1 and m, Equation (14) has a unique local solution curve $(q(\omega), p(\omega))$ (i.e., marginal stability curve). The marginal stability curve divides the (q, p) plane into two parts: meeting stability margin and not meeting stability margin. The curve is the contour. Then, once an appropriate work point in the contour is obtained, the controller parameters can be calculated. The method of choosing a work point is shown after the analysis of the parameter k, because the parameter k can influence the choosing method.

Next, the function of the controller parameters (h_0, h_1, m, k) is analyzed, and the method for obtaining them is shown.

h_0 and h_1 are coefficients of the desired dynamic equation. They are chosen based on the requirements of control system, such as settling time, overshooting, and so on. Because the desired dynamic equation is a second-order system, h_0 and h_1 can be calculated according to the second-order system, as follows:

$$h_1 = 2\zeta\omega_n = 8/t_{sd}, h_0 = h_1^2/4\zeta^2. \tag{15}$$

where t_{sd} is the desired settling time; ζ is the damping of desired dynamic system; and ω_n is the natural frequency of desired dynamic system.

In order to make the overshooting as small as possible and make the settling time as short as possible, $\zeta = 1$ is chosen. Considering the error between the actual dynamic and the desired dynamic, Equation (15) becomes

$$h_1 = \frac{8 \sim 25}{t_{sd}}, h_0 = h_1^2/4. \tag{16}$$

The stability margin increases with the increasing of the attenuation index m. It is well-known that there is a trade-off between performance and robustness [26,27]. Therefore, choosing an appropriate m is important to avoid the conflict with both h_0 and h_1. According to our experience, the reasonable selecting region of m is generally $(0.2, 2)$. One other thing to note is that a greater m is needed when the model is imprecise.

Combine Equation (2) with Equation (5) and do a Laplace transform, and the following equation is obtained:

$$\hat{f} = \frac{k}{s+k} f. \tag{17}$$

Its derivation is shown in Appendix B.

As shown in Equation (17), the response rate of the disturbance observer speeds up with k increasing. So, the work point should be chosen nearby the q-axis in order to make k as large as possible because $k = q/p$ in the (q, p) plane.

The work point is chosen as follows.

First, substitute $q = 0$ into Equation (14), and the following equation is obtained.

$$\begin{cases} (h_0 - 2m\omega h_1) \\ \quad = -\frac{m\sin(\varphi_0(m,\omega)) + \cos(\varphi_0(m,\omega))}{M_0(\varphi_0(m,\omega))} \\ \omega h_1 p = \frac{\sin(\varphi_0(m,\omega))}{M_0(\varphi_0(m,\omega))} \end{cases}. \tag{18}$$

Solve Equation (18), and $p_{q=0}$ and $\omega_{q=0}$ can be obtained.

Then, define

$$p^* = p_{q=0}/(10 \sim 50) \tag{19}$$

and substitute p^* into Equation (14), so q^* and ω^* can be obtained. The point (q^*, p^*) is the work point in the (q, p) plane.

Finally, substitute p^* and q^* into Equation (13), and the controller parameters are obtained.

The steps of setting the controller parameters are shown as follows:

(1) Obtain the system model and choose proper h_0, h_1 and m values according to the requirements of system;
(2) Solve Equation (18), and then get $p_{q=0}$ and $\omega_{q=0}$;
(3) Get p^* from Equation (19), substitute p^* into Equation (14), and then get q^* and ω^*;
(4) Substitute p^* and q^* into Equation (13) to calculate the controller parameters. If there are closed-loop poles outside of the sector area, decrease both h_0 and h_1 simultaneously or only m, and then turn to step (2); otherwise, continue;
(5) Do the step response and calculate the settling time and overshooting. If the settling time is not met, then increase both h_0 and h_1 or decrease m, and turn to step (2); if the overshooting is too great, then decrease both h_0 and h_1 or increase m, and turn to step (2); otherwise, continue;
(6) End.

3. Illustrative Examples

To demonstrate the application of the 2DOF PID tuning method proposed in the previous sections, now the simulation results for different processes are presented using MATLAB. In this section, firstly the previous theoretical analysis of the controller parameters is verified with simulation. Then, compared with Panagopoulos' method [15], the proposed method is effective and superior.

3.1. PID Controller Parameters Analysis with Simulation

In this subsection, the influence of the controller parameters (m, k, h_0, h_1) will be analyzed through simulation.

Consider a process given by $G = \frac{1}{(s+1)^3}$.

If the settling time is less than 10 s, the desired dynamic coefficient (h_0, h_1) can be calculated from Equation (16). $h_1 = 1.5$ and $h_0 = 0.5625$ are chosen. The m contours are shown in Figure 4 where m is equal to 0.5, 0.6, 0.7, and 0.8 respectively.

As shown in Figure 4, the greater the m, the closer to origin the contour. Parameter ω increases in the counter-clockwise direction. In order to analyze the influence of parameter m and parameter k on the behavior of the closed-loop time response and the frequency response, seven points A, B, C, D, E, F, and G are chosen. Among them, points C, D, E, and F are characterized by the same stability margin $m = 0.6$, and points A, B, C and G are characterized by roughly the same disturbance observer coefficient k, which is big enough. The coordinates of the seven points in the (q, p) plane are listed in Table 1.

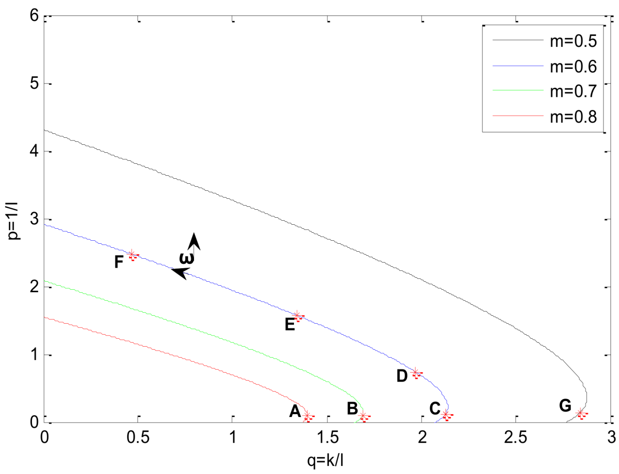

Figure 4. The m contours.

Table 1. The coordinates of points from A–G in the (q, p) plane.

	A	B	C	D	E	F	G
q	1.398	1.689	2.128	1.967	1.342	0.4648	2.84
p	0.0895	0.0903	0.1106	0.7344	1.567	2.475	0.1279

The closed-loop time response and the closed-loop frequency response of process $G(s)$ for points C, D, E, and F are shown in Figures 5–7, which show the influence of parameter k. In the time response case, load disturbance is introduced at $t = 50$ s.

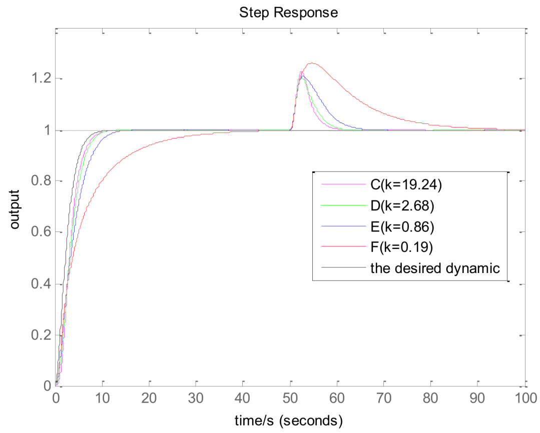

Figure 5. The time response of process $G(s)$ for points C, D, E, and F. Load disturbance is introduced at $t = 50$ s.

On the one hand, from the simulation results of Figure 5, it can be observed that the setpoint response is closer to the desired dynamic with the increasing k. Furthermore, the influence of k is weakened when k adds up to certain values that are too great. In Figure 6, the frequency characteristic of the low-frequency range is closer to the desired dynamic with the increasing k. On the other hand, in Figure 5, the load disturbance response is also improved with the increasing k. The reason is that the integral coefficient k_i enlarges with the increasing k. In addition, the influence of k is weakened when k adds up to certain high values. In Figure 7, the amplitude of the low-frequency range is lower with the increasing k.

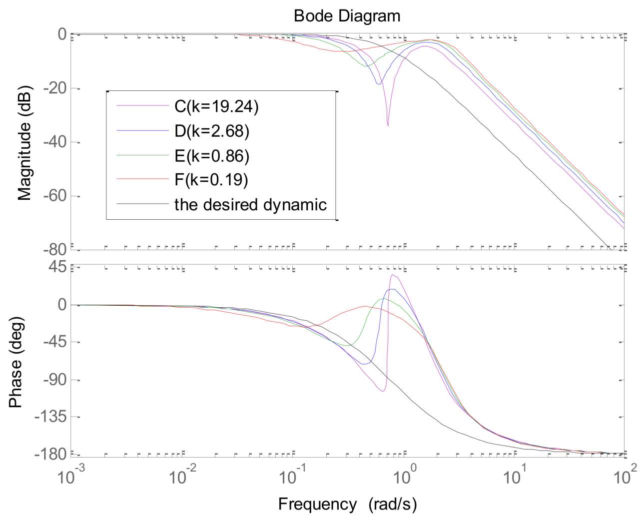

Figure 6. The closed-loop setpoint frequency response of the process $G(s)$ for points C, D, E, and F.

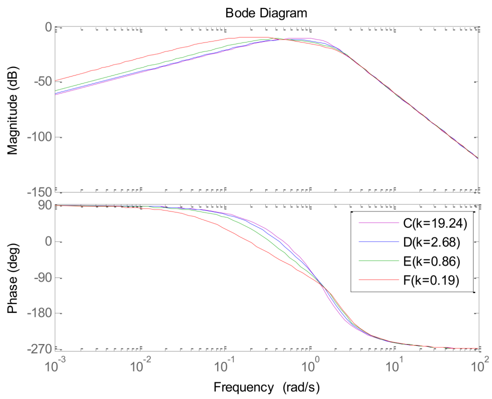

Figure 7. The closed-loop load disturbance frequency response of the process $G(s)$ for points C, D, E, and F.

The closed-loop time response and the closed-loop frequency response of process $G(s)$ for points A, B, C, and G are shown in Figures 8–10 from which the influence of parameter m can be seen. In the time response case, the load disturbance is introduced at $t = 25$ s.

On the one hand, in Figure 8, the setpoint response rate is slower with the increasing m. In Figure 9, the magnitude of the low-frequency range is also closer to 0 dB. On the other hand, in Figure 8, the load disturbance response is deteriorated with the increasing m. In Figure 10, it is shown that the magnitude of the low-frequency range is higher with a greater m. The above phenomena are a result of the stability margin increasing with the increasing m, and there is a trade-off between performance and robustness.

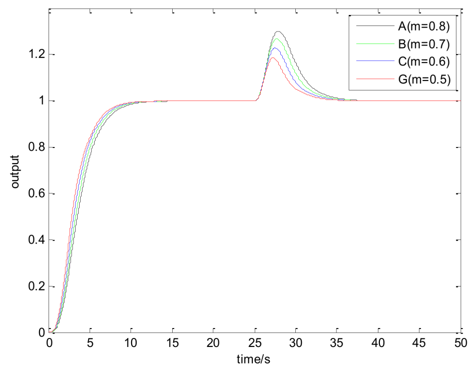

Figure 8. The time response of process $G(s)$ for points A, B, C, and G. Load disturbance is introduced at $t = 25$ s.

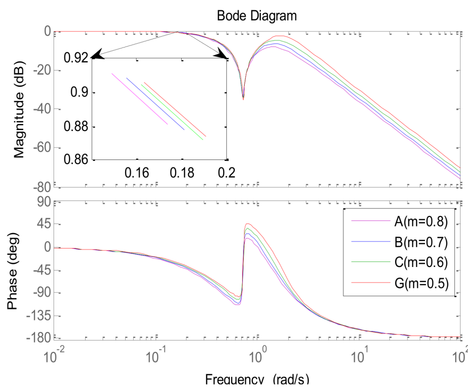

Figure 9. The closed-loop setpoint frequency response of the process $G(s)$ for points A, B, C, and G.

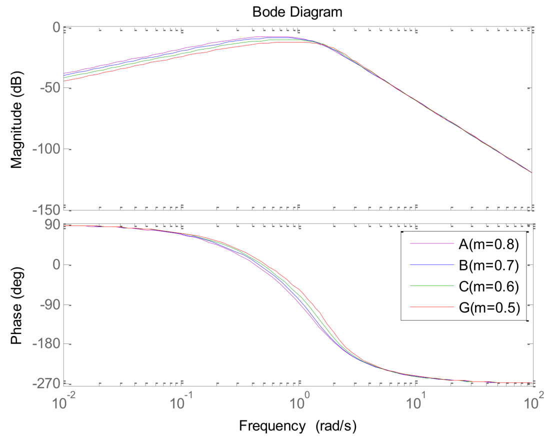

Figure 10. The closed-loop load disturbance frequency response of the process $G(s)$ for points A, B, C, and G.

To demonstrate the influence of h_0 and h_1, the same m and = different (h_0, h_1) are chosen, and then, the h contours are depicted in Figure 11 where $m = 0.6$ and (h_0, h_1) are respectively equal to $(0.36, 1.2)$, $(0.5625, 1.5)$, and $(0.81, 1.8)$.

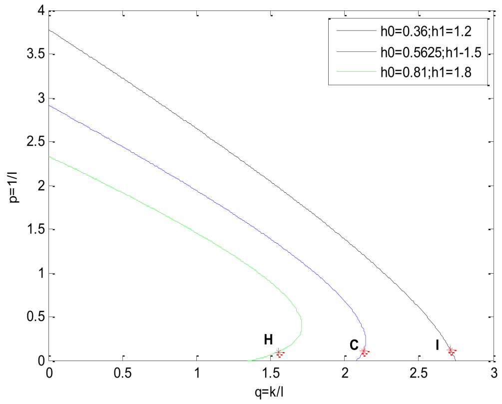

Figure 11. The h contours.

As shown in Figure 11, the h contour is closer to the origin with the increasing of both h_0 and h_1. To analyze the influence of both h_0 and h_1, three points H, C, and I were chosen. The coordinates of these points in the (q, p) plane are listed in Table 2.

Table 2. The coordinate of points H, C, and I in the (q, p) plane.

	H	C	I
q	1.546	2.128	2.712
p	0.0927	0.1106	0.1251

The closed-loop time response and the closed-loop frequency response of process $G(s)$ for points H, C, and I are shown in Figures 12 and 13, which show the influence of the parameters h_0 and h_1. In the time response case, the load disturbance is introduced at t = 25 s.

On the one hand, Figure 12 shows that the setpoint time response speeds up by increasing both h_0 and h_1. From Figure 13, it can be observed that the magnitude of the low-frequency range is closer to 0 dB. The above phenomena result from the fact that the desired dynamic is faster with greater h_0 and

h_1. On the other hand, Figure 12 also shows that the load disturbance response returns to the target faster, and the peak is higher with greater h_0 and h_1.

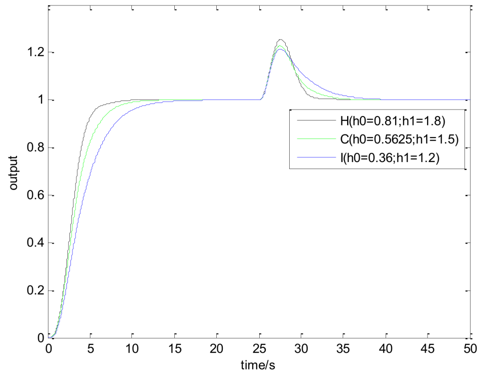

Figure 12. The closed-loop time response of process $G(s)$ for points H, C, and I.

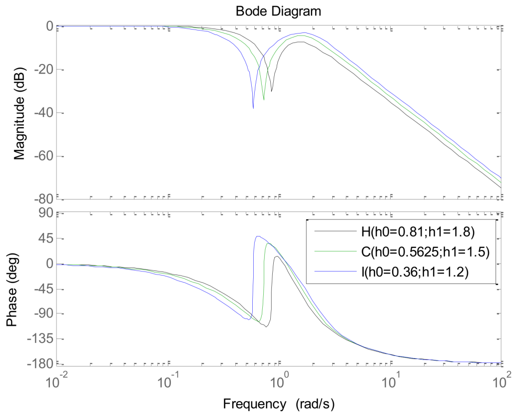

Figure 13. The closed-loop setpoint frequency response of the process $G(s)$ for points H, C, and I.

The simulation results of the nine points A~I have not only shown the influence of the parameters (m, k, h_0, h_1), but also prove that the specified stability margin can be met as follows. All the closed-loop poles of points from A to I are shown in Table 3, and it can be seen that all the closed-loop poles lie in the specified sector region. From Table 3, it can be also observed that among all the m_n corresponding to the poles, the smallest is equal to the previous specified m.

Table 3. The closed-loop poles and the corresponding smallest m of all points A~ I.

	The Closed-Loop Poles				**The Smallest m_n**
A	−0.868 + 1.085i	−0.868 − 0.085i	−0.632 + 0.089i	−0.632 − 0.089i	0.8
B	−0.8456 + 1.2079i	−0.8456 − 1.2079i	−0.6544 + 0.0939i	−0.6544 − 0.0939i	0.7
C	−0.8316 + 1.3859i	−0.8316 − 1.3859i	−0.6684 + 0.1071i	−0.6684 − 0.1071i	0.6
D	−0.9996 + 1.666i	−0.9996 − 1.666i	−0.5004 + 0.2067i	−0.5004 − 0.2067i	0.6
E	−1.1377 + 1.896i	−1.1377 − 1.896i	−0.3623 + 0.152i	−0.3623 − 0.152i	0.6
F	−1.2462 + 2.0772i	−1.2462 − 2.0772i	−0.3947	−0.1129	0.6
G	−0.8145 + 1.6289i	−0.8145 − 1.6289i	−0.6855 + 0.1083i	−0.6855 − 0.1083i	0.5
H	−0.6852 + 1.142i	−0.6852 − 1.142i	−0.8148 + 0.2052i	−0.8148 − 0.2052i	0.6
I	−0.9654 + 1.6088i	−0.9654 − 1.6088i	−0.6266	−0.4426	0.6

3.2. Comparison with Panagopoulos' Method

This section will present the results compared with Panagopoulos' method [15] to show the superiority of the proposed tuning method.

The control law of Panagopoulos' method is as follows:

$$\begin{cases} u(t) = k(b_1 y_r'(t) - y(t)) + \frac{k}{T_i}\int\limits_0^t (y_r'(\tau) - y(\tau))d\tau \\ \quad +kT_d\left(-\frac{dy(t)}{dt}\right) \\ y_r'(s) = \frac{1}{(1+sT_{sp})} y_r(s) \end{cases}$$

Under the condition that $M_s = 2$, eight different processes [15] serve as examples. The eight processes cover high–order process, non–minimum phase process, time–delay process, and integrating process, which are listed as follows:

$$G_1 = \frac{1}{s(s+1)^3}$$

$$G_2 = \frac{e^{-5s}}{(s+1)^3}$$

$$G_3 = \frac{1}{(s+1)(0.2s+1)(0.04s+1)(0.008s+1)}$$

$$G_4 = \frac{1}{(s+1)^4}$$

$$G_5 = \frac{1}{(s+1)^5}$$

$$G_6 = \frac{1}{(s+1)^6}$$

$$G_7 = \frac{1}{(s+1)^7}$$

$$G_8 = \frac{-2s+1}{(s+1)^3}$$

Table 4 collects the related parameters of the DDE−GFM, including h_0, h_1, m, k_p, k_i, k_d, and b, and the related parameters of Panagopoulos' method, which covers k, T_i, T_d, b_1 and T_{sp}.

Table 5 presents the position of the work point in the (q, p) plane of the DDE−GFM and the control signal and time response of the two methods. On the one hand, it can be seen that the work points of all the processes are positive, as well as the nearby $q-$axis, which can make parameter k large enough. Consequently, the estimation of the total disturbance is more precise. On the other hand, the settling time of the DDE−GFM for G_3 and G_8 is obviously shorter than that of Panagopoulos' method. Moreover, compared with Panagopoulos' method, the overshooting of the DDE−GFM is substantially smaller, except for G_3 for which the overshooting is zero.

Table 4. The related parameters of the DDE−GFM and Panagopoulos' method.

	DDE–GFM							**Panagopoulos' Method**				
	h_0	h_1	m	k_p	k_i	k_d	b	k	T_i	T_d	b_1	T_{sp}
G_1	0.0625	0.5	0.35	0.6999	0.0863	1.4594	0.69	0.68	4.5	2.27	0	0.08
G_2	0.25	1	0.5	0.5495	0.1365	0.5608	0.5458	0.555	3.21	1.74	0	1.61
G_3	16	8	0.35	44.767	88.768	5.7393	44.384	43.13	0.189	0.13	0	0.81
G_4	0.49	1.4	0.35	2.1591	0.7389	1.6449	2.1112	2.27	1.91	0.98	0	0.53
G_5	0.25	1	0.3	1.6934	0.4118	1.8324	1.647	1.47	2.33	1.25	0	0.72
G_6	0.16	0.8	0.3	1.3189	0.2605	1.7107	1.3024	1.15	2.74	1.49	0	0.97
G_7	0.2025	0.9	0.4	0.9721	0.2149	1.1373	0.9549	0.982	3.14	1.73	0	1.24
G_8	0.64	1.6	0.85	0.5757	0.2276	0.3722	0.5691	0.542	2.07	0.79	0	1.03

Table 5. The simulation results covering the position of the work point in the (q, p) plane and the control signal and time response comparing the DDE−GFM and Panagopoulos' method.

Process	Work Point in (q, p) Plane	Control Signal of DDE−GFM and Panagopoulos' Method	Time Response of DDE−GFM and Panagopoulos' Method
G_1	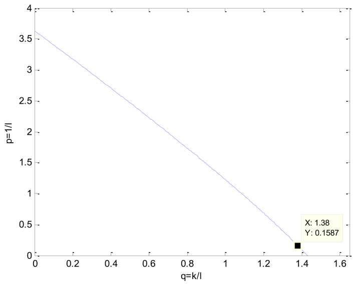	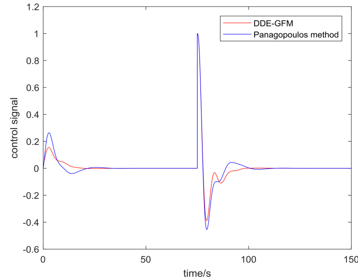	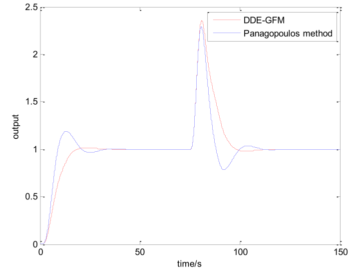
G_2	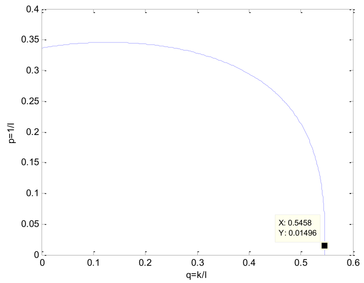	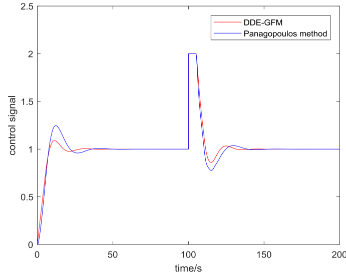	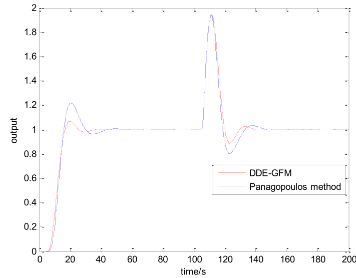
G_3	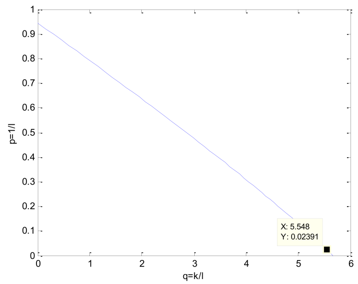	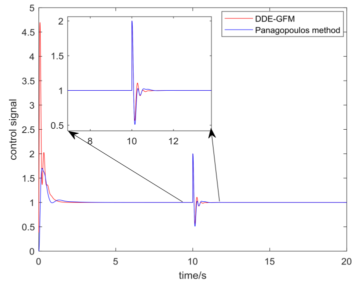	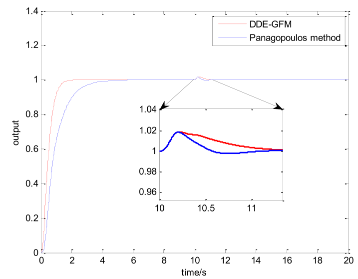

Table 5. *Cont.*

Process	Work Point in (q, p) Plane	Control Signal of DDE−GFM and Panagopoulos' Method	Time Response of DDE−GFM and Panagopoulos' Method
G_4	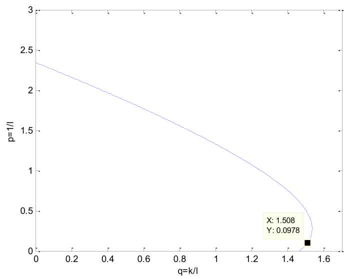	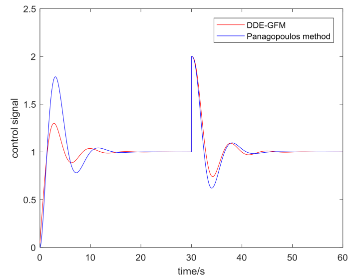	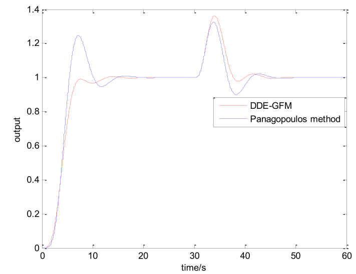
G_5	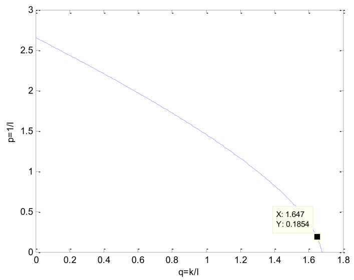	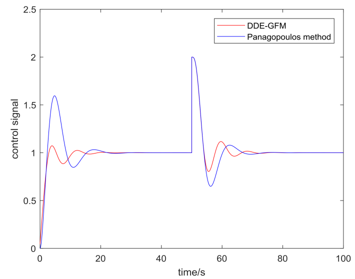	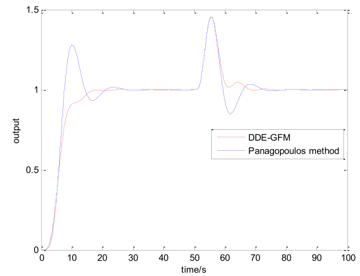
G_6	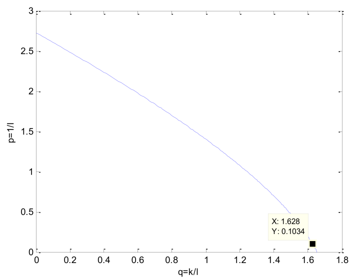	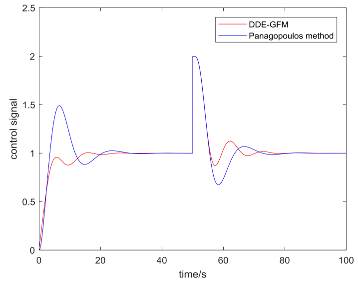	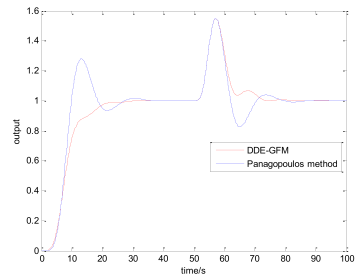

Table 5. *Cont.*

Process	Work Point in (q, p) Plane	Control Signal of DDE−GFM and Panagopoulos' Method	Time Response of DDE−GFM and Panagopoulos' Method
G_7	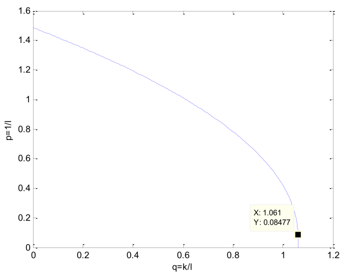	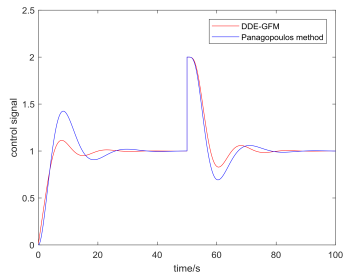	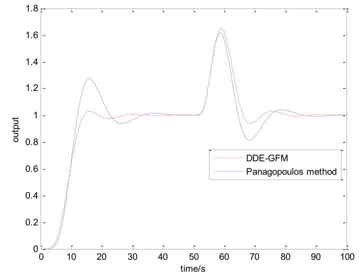
G_8	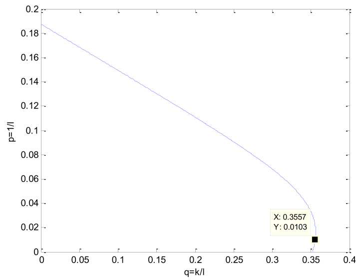	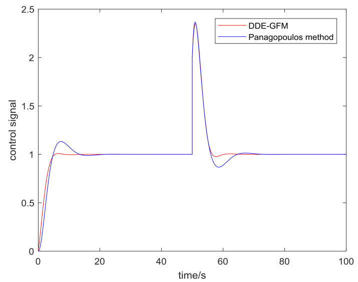	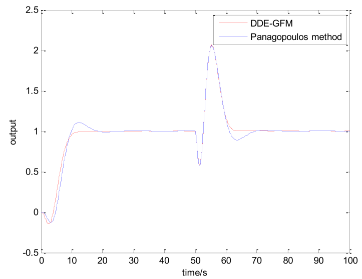

Further details of the simulation results can be seen in Table 6, which includes the settling time, the overshooting, the integral absolute error (IAE), and the maximum sensitivity M_s of the two methods. It can be seen that the settling time is shortened by 15~60%. Except for G_3 for which the overshooting is zero, the overshooting of the other processes are all reduced by more than 70%. Furthermore, the overshooting of G_5, G_6, and G_8 are even directly reduced to zero. The IAE index of the two methods for each process are approximately equal except for that of G_3 for which the IAE index is approximately zero. In addition, the maximum sensitivity M_s of two methods for all the processes are equal to 2.

Table 6. The performance for the DDE−GFM and Panagopoulos' method.

	Methods	Settling Time (s)	Overshooting (%)	IAE	M_s
G_1	DDE−GFM Panagopoulos'	16.952 28.678	1.56 16.77	11.96 9.252	2 2
G_2	DDE−GFM Panagopoulos'	24.232 39.392	6.89 21.68	8.6902 9.1035	2 2
G_3	DDE−GFM Panagopoulos'	1.4 3.344	0 0	0.0113 0.0058	2 2
G_4	DDE−GFM Panagopoulos'	11.368 13.022	0.57 23.47	1.441 1.3511	2 2
G_5	DDE−GFM Panagopoulos'	15.468 19.429	0 27.24	2.4522 2.749	2 2
G_6	DDE−GFM Panagopoulos'	20.829 25.273	0 27.39	3.8433 4.1654	2 2
G_7	DDE−GFM Panagopoulos'	24.521 30.931	2.81 26.72	5.2316 5.5291	2 2
G_8	DDE−GFM Panagopoulos'	11.003 17.027	0 10.19	5.67 6.1111	2 2

4. Conclusions

A new tuning method is proposed for a two-degree-of-freedom PID controller, which combines the advantages of the DDE and the GFM. Firstly, choose appropriate h_0, h_1, and m. Secondly, calculate $p_{q=0}$ using Equation (18). Thirdly, calculate p^* using Equation (19), and then substitute p^* into Equation (14) to calculate q^*. Finally, substitute (q^*, p^*) into Equation (13), and then, calculate the controller parameters. The main advantage of the proposed method is that the desired dynamic and the stability margin can be guaranteed simultaneously. In addition, a set of formulas were obtained to calculate the controller parameters. Moreover, the method can perform a fast setpoint response with minimal overshooting. Compared with Panagopoulos' method, the proposed method is more effective and superior.

Acknowledgments: National Key Technology Support Program (2015BAF30B00)

Author Contributions: Donghai Li and Xiaoqiang Yan conceived and designed the experiments; Xinxin Wang performed the experiments; Xinxin Wang and Li Sun analyzed the data; Li Sun contributed reagents/materials/analysis tools; Xinxin Wang wrote the paper.

Conflicts of Interest: The authors declare no conflict of interest.

Appendix

From Equation (5), the following equation is obtained:

$$u = -(\xi + kz_2)/l - \dot{\xi}/kl. \tag{A1}$$

Substitute $\hat{f} = \xi + kz_2$ into Equation (4), and the following equation is obtained:

$$u = -\frac{\xi + kz_2}{l} - \frac{h_0(z_1 - y_r) + h_1 z_2}{l}. \tag{A2}$$

Compare Equation (A1) with Equation (A2); the following equation is obtained:

$$\dot{\xi} = kh_0(z_1 - y_r) + kh_1 z_2. \tag{A3}$$

Integrate Equation (A3), and the following equation is obtained:

$$\xi = kh_0 \int (z_1 - y_r)dt + kh_1 z_1. \tag{A4}$$

Substitute Equation (A4) into Equation (A2), and define $e = y_r - z_1$; the following equation is obtained:

$$\begin{aligned} u &= -\frac{kh_0 \int (z_1 - y_r)dt + kh_1 z_1 + kz_2}{l} - \frac{h_0(z_1 - y_r) + h_1 z_2}{l} \\ &= \frac{(h_0 + kh_1)e + kh_0 \int edt + (h_1 + k)\dot{e} - kh_1 y_r}{l} \end{aligned} \tag{A5}$$

Appendix

Take the derivative of the first equation in Equation (5), and the following equation is obtained:

$$\dot{\hat{f}} = \dot{\xi} + k\dot{z}_2 \tag{A6}$$

Substitute the second equation in Equation (5) and the second equation in Equation (2) into Equation (A6), and the following equation is obtained:

$$\dot{\hat{f}} = -k(\xi + kz_2) + kf \tag{A7}$$

Substitute the second equation in Equation (5) into Equation (A7), and the following equation is obtained:

$$\dot{\hat{f}} = -k\hat{f} + kf \tag{A8}$$

Take the Laplace transform of Equation (A8), and the following equation is obtained:

$$\hat{f} = \frac{k}{s + k} f \tag{A9}$$

References

1. Astrom, K.J.; Hagglund, T. The future of PID control. *Control Eng. Pract.* **2001**, *9*, 1163–1175. [CrossRef]
2. Ang, K.H.; Chong, G.; Li, Y. PID control system analysis, design, and technology. *IEEE Trans. Control Syst. Technol.* **2005**, *13*, 559–576.
3. Åström, K.J.; Hägglund, T. *Advanced PID Control*; ISA, Research Triangle Park: Durham, NC, USA, 2006.
4. Araki, M.; Taguchi, H. Two-degree-of-freedom PID controllers. *Int. J. Control Autom. Syst.* **2003**, *1*, 401–411.
5. Middleton, R.H. Trade-offs in linear control system design. *Automatica* **1991**, *27*, 281–292. [CrossRef]
6. De Moor, B.; David, J.; Vandewalle, J.; de Moor, M.; Berckmans, D. Trade−offs in linear control system design: A practical example. *Optim. Control Appl. Methods* **1992**, *13*, 121–144. [CrossRef]
7. Horowitz, I.M. *Synthesis of Feedback Systems*; Academic Press: New York, NY, USA, 1963.
8. Dinca, M.P.; Gheorghe, M.; Galvin, P. Design of a PID controller for a PCR micro reactor. *IEEE Trans. Educ.* **2009**, *52*, 116–125. [CrossRef]
9. Viteckova, M.; Vitecek, A. 2DOF PI and PID controllers tuning. *IFAC Proc. Vol.* **2010**, *43*, 343–348. [CrossRef]
10. Morari, M. *Robust Process Control*; Prentice Hall: Englewood Cliffs, NJ, USA, 1989.

11. Sutikno, J.P.; Aziz, B.A.; Yee, C.S.; Mamat, R. A new tuning method for two-degree-of-freedom internal model control under parametric uncertainty. *Chin. J. Chem. Eng.* **2013**, *21*, 1030–1037. [CrossRef]
12. Jin, Q.B.; Liu, Q. Analytical IMC−PID design in terms of performance/robustness tradeoff for integrating processes: From 2-Dof to 1-Dof. *J. Process Control* **2014**, *24*, 22–32. [CrossRef]
13. Xing, Z.; Zhu, Q.; Ding, Y. Two-degree-of-freedom IMC−PID design of missile servo system based on tuning gain and phase margin. *J. Harbin Eng. Univ.* **2006**, *27*, 404–407.
14. Alfaro, V.M.; Vilanova, R.; Arrieta, O. Maximum Sensitivity Based Robust Tuning for Two-Degree-of-Freedom Proportional-Integral Controllers. *Ind. Eng. Chem. Res.* **2010**, *49*, 5415–5423. [CrossRef]
15. Panagopoulos, H.; Astrom, K.J.; Hagglund, T. Design of PID controllers based on constrained optimisation. *IEE Proc. Control Theory Appl.* **2002**, *149*, 32–40. [CrossRef]
16. Wang, W.; Li, D.; Gao, Q.; Wang, C. Two-degrees-of-freedom PID controller tuning method. *J. Tsinghua Univ.* **2008**, *48*, 1962–1966.
17. Weijie, W. *The PID Parameter Tuning Method and Its Application in Thermal Control*; Tsinghua University: Beijing, China, 2009.
18. Min, Z. Simulation analysis of PID control system based on desired dynamic equation. In Proceedings of the 2010 8th World Congress on Intelligent Control and Automation (WCICA), Jinan, China, 7–9 July 2010; University of Science and Technology: Beijing, China, 2010.
19. Li, D.; Xue, Y.; Wang, W.; Sun, L. Decentralized PID controller tuning based on desired dynamic equations. In Proceedings of the 19th World Congress The International Federation of Automatic Control, Cape Town, South Africa, 24–29 August 2014; pp. 5802–5807.
20. Zhang, Y.; Li, D.; Lao, D. Smith predictor in the DDE application. In Proceedings of the 2012 24th Chinese Control and Decision Conference (CCDC), Taiyuan, China, 23–25 May 2012; pp. 2346–2351.
21. Tornambe, A.; Valigi, P. Decentralized controller for the robust stabilization of a class of MIMO dynamical systems. *J. Dyn. Syst. Meas. Control Trans. ASME* **1994**, *116*, 293–304. [CrossRef]
22. Hu, Z.; Wang, J.; Li, D.; Qin, J. Application of Desired Dynamic Equation method in simulation of four-tank system. In Proceedings of the 2012 International Conference on Systems and Informatics (ICSAI), Yantai, China, 19–20 May 2012; pp. 366–370.
23. Hu, Y.; Li, D.; Zhu, M.; Gu, T. Active control of combustion oscillations based on desired dynamic equation. In Proceedings of the 2010 International Conference on Control Automation and Systems (ICCAS), Gyeonggi-do, Korea, 27–30 October 2010; pp. 787–791.
24. Laijiu, C. *Automatic Control Principle and Application for Thermal Process*; Water Conservancy and Electric Power Press: Beijing, China, 1982.
25. Xianyong, Y. *Automatic Control for Thermal Process*, 2nd ed.; Tsinghua University Press: Beijing, China, 2008.
26. Alfaro, V.M.; Vilanova, R. Simple robust tuning of 2DoF PID controllers from a performance/robustness trade−off analysis. *Asian J. Control* **2013**, *15*, 1700–1713. [CrossRef]
27. Alfaro, V.M.; Vilanova, R.; Mendez, V.; Lafuente, J. Performance/robustness tradeoff analysis of PI/PID servo and regulatory control systems. In Proceedings of the 2010 IEEE International Conference on Industrial Technology, Vina del Mar, Chile, 14–17 March 2010; pp. 111–116.